Phase portrait analysis of a cantilevered piezoelectric-electromagnetic energy harvester

Ngoc-Hung Nguyen[1,2], Van-Manh Nguyen[3], Ngoc-Linh Nguyen[4], Tuan-Anh Tran[4,5*]

Abstract: This paper investigates a piezoelectric-electromagnetic hybrid energy harvester (PEM-HEH) which has only been developed recently where a linear electromagnetic harvester is attached to the free end of a cantilevered piezoelectric bimorph. First, the electromechanical model of PEM-HEH is introduced based on Euler–Bernoulli theory and Lagrange's equations. It is demonstrated the coupling between the linear transverse motion of the piezoelectric bimorph and the nonlinear axial motion of the magnet inside the electromagnetic harvester. It turns out that the combination of two linear harvesters leads to a frequency-doubling effect in a nonlinear system. Next, a sample test is implemented to verify the characteristics of the nonlinearity of the system in phase portrait. Finally, relevant conclusions could be drawn.

Keywords: Cantilevered piezoelectric bimorph, linear electromagnetic harvester, piezoelectric-electromagnetic hybrid energy harvester, frequency-doubling, phase portrait.

1. Introduction

Vibration energy harvesting has become a sustainable solution for powering low-power electronics and wireless sensors by converting ambient vibrations into usable electrical energy (Ahmad & Khan, 2020; Erturk & Inman, 2011). Among various conversion mechanisms, piezoelectric and electromagnetic methods are widely used due to their high efficiency and flexible integration.

However, a major limitation of linear piezoelectric energy harvesters is their narrow operating bandwidth; they only provide optimal performance when the ambient vibration frequency matches the device's resonance frequency (Ahmad & Khan, 2020; Erturk & Inman, 2011). This makes them ineffective in environments with variable vibration frequencies. To overcome this, recent research has focused on developing nonlinear energy harvesters. For instance, multistable systems (Fang et al., 2022) and mechanical end stops (Zheng et al., 2014) have been shown to broaden the operating frequency range and increase oscillation amplitude, thereby enhancing energy harvesting efficiency. Furthermore, phenomena like parametric resonance (Fan et al., 2024) and stochastic resonance (Zheng et al., 2014) offer improved efficiency for small and random excitations.

A promising approach is the combination of piezoelectric and electromagnetic mechanisms into hybrid energy harvesters (Li et al., 2014). By combining the power density of piezoelectricity and the efficient low-frequency voltage generation of electromagnetism, this system achieves higher power output across a broader frequency band (Li et al., 2014). Hybrid harvesters can be designed for complex environments with fluid-induced vibrations like vortex-induced vibrations and random excitations.

This study presents a hybrid piezoelectric-electromagnetic energy harvester (PEM–HEH) model, designed to capture energy from low-frequency, broadband vibrations. Using Euler-Bernoulli beam theory, we developed a distributed-parameter electromechanical model that accurately simulates the coupled mechanisms. This work serves as a theoretical foundation for predicting and optimizing performance, building upon existing research on frequency-doubling and squared-amplitude effects were first systematically analyzed (Hung et al., 2025). The goal is to design more efficient energy harvesters for future applications.

2. Modelling of pem–heh

As depicted in Figure 1.a (Hung et al., 2025), the model of the bimorph is a cantilever beam with a transverse displacement w_{rel} at the neutral axis which is relative to its base, and a rotation angle φ. The masses $M_f, m_g,$ and M_t are the rigid bodies with the coordinates of the center of mass $(x_f, z_f), (x_g, z_g), (x_t, z_t)$ respectively, and their rotation angle equal are assumed to be the same as that of the bimorph at the free end, namely φ_L. Accordingly, $w_L(t)$ and $\varphi_L(t)$ are the deflection and slope of the bimorph at $x=L$

[1]Faculty of Engineering Mechanics and Automation, VNU University of Engineering and Technology, Vietnam National University, Vietnam
[2]Department of Science and Technology of Thanh Hoa Province, Vietnam
[3]Faculty of Mechanical Engineering, Hanoi University of Civil Engineering, Vietnam
[4]Faculty of Mechanical Engineering, Thuyloi University, Vietnam
[5]Graduate University of Science and Technology, Vietnam Academy of Science and Technology, Hanoi, Vietnam
* Corresponding author
Received 15th Sep. 2025
Accepted 12th Dec. 2025
Publication date 31st Dec. 2025

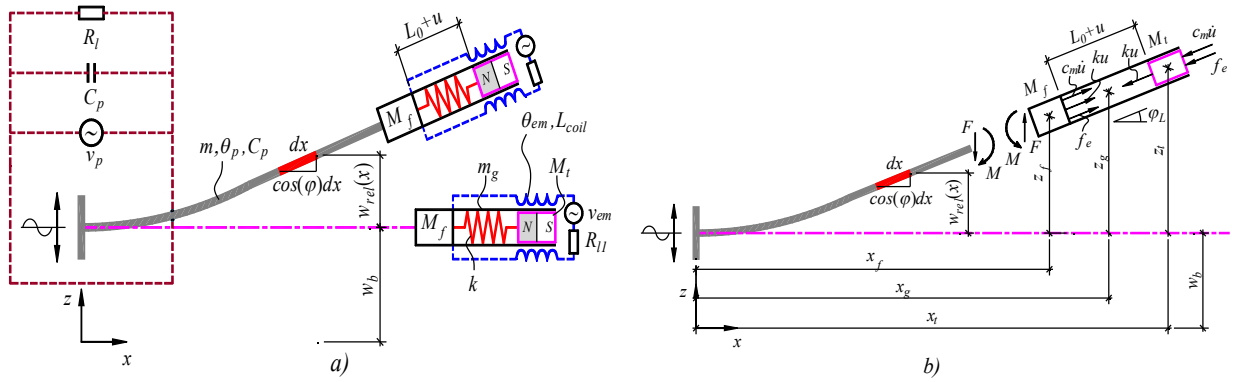

Figure 1. a) Electromechanical model of PEM-HEH; b) Deformed cantilevered bimorph and free body diagram

$$w_L(t) = w_{rel}(L,t); \varphi_L(t) = \varphi(L,t) = \frac{\partial w_{rel}}{\partial x}(L,t) \tag{1}$$

The PEM–HEH is subjected to a harmonic excitation at the base of the bimorph, i.e.

$$w_b(t) = W_0 \sin(\omega t) \tag{2}$$

where W_0 is the base displacement amplitude, ω is the excitation frequency. In the subsystem, the geometrical relationship of the coordinates of the center of masses M_f, m_g, and M_t are

$$\begin{aligned} x_f(t) &= \int_0^L \cos\varphi(x,t)dx; z_f = w_b + w_L; \\ x_g &= \int_0^L \cos\varphi(x,t)dx + \frac{L_g}{2}\cos\varphi_L; z_g = w_b + w_L + \frac{L_g}{2}\sin\varphi_L; \\ x_t &= \int_0^L \cos\varphi(x,t)dx + (L_0 + u(t))\cos\varphi_L; \\ z_t(t) &= w_b + w_L + (L_0 + u(t))\sin\varphi_L \end{aligned} \tag{3}$$

where $u(t)$ is the axial displacement mass M_t. Using the free body diagram as depicted in Figure 1.b where the subsystem and the bimorph are divided into two main bodies, then the resultant reactions at the connecting joint can be represented by a force F and a moment M acting on the subsystem and the bimorph. Meanwhile, $f_e, c_m\dot{u}, ku$ are the magnetic, mechanical damping force and spring forces acting on the mass M_t along with the direction u, respectively. First, consider the kinetic energy T of the subsystem including three masses M_f, m_g, and M_t, one has

$$T = \frac{M_f}{2}(\dot{z}_f^2 + \dot{x}_f^2) + \frac{M_t}{2}(\dot{z}_t^2 + \dot{x}_t^2) + \frac{m_g L_g}{2}(\dot{z}_g^2 + \dot{x}_g^2) + \frac{m_g L_g^3}{24}\dot{\varphi}_L^2 \tag{4}$$

Using (4), the motion equations of the subsystem derived from the Lagrange's equations read

$$\frac{d}{dt}\frac{\partial T}{\partial \dot{w}_L} - \frac{\partial T}{\partial w_L} = F \tag{5}$$

$$\frac{d}{dt}\frac{\partial T}{\partial \dot{\varphi}_L} - \frac{\partial T}{\partial \varphi_L} = M \tag{6}$$

$$\frac{d}{dt}\frac{\partial T}{\partial \dot{u}} - \frac{\partial T}{\partial u} = -(c_m\dot{u} + ku + \theta_{em}I_{em}) \tag{7}$$

$$L_{coil}\dot{I}_{em} + R_{l1}I_{em} = \theta_{em}\dot{u} \tag{8}$$

On the other hand, based on Euler-Bernoulli beam theory, the governing equations of the bimorph subjected to base excitation w_b are (Erturk and Inman, 2011):

$$YI\frac{\partial^4 w_{rel}}{\partial x^4} + c_s I\frac{\partial^5 w_{rel}}{\partial x^4 \partial t} + m\frac{\partial^2 w_{rel}}{\partial t^2} - \theta_p v_p\left[\frac{d\delta(x)}{dx} - \frac{d\delta(x-L)}{dx}\right] = -m\frac{\partial^2 w_b}{\partial t^2} \tag{9}$$

$$C_p\frac{dv_p}{dt}+\frac{v_p}{2R_l}+\frac{\theta_p}{2}\int_0^L\frac{\partial^3 w_{rel}}{\partial x^2\partial t}dx=0 \quad (10)$$

where c_s is the strain-rate damping coefficient of bimorph, YI is the bending stiffness, m is the mass per unit length, C_p is the internal capacitance, θ_p is the piezoelectric coupling coefficient, and $\delta(x)$ is the Dirac delta function, respectively. The force F and the moment M applied to the free end of the bimorph can be expressed using boundary conditions at the free end $x=L$

$$F=YI\frac{\partial^3 w_{rel}}{\partial x^3}(L,t)+c_sI\frac{\partial^4 w_{rel}}{\partial x^3\partial t}(L,t) \quad (11)$$

$$M=-YI\frac{\partial^2 w_{rel}}{\partial x^2}(L,t)-c_sI\frac{\partial^3 w_{rel}}{\partial x^2\partial t}(L,t) \quad (12)$$

As we can see in Eqs. (11), (12), the force F and the moment M are dependent on $w_{rel}(x,t)$. Thus, six equations (5)-(10) perform a differential equation systems for 6 variables: $w_{rel}(x,t), w_L(t), \varphi(t), u(t), v_p(t)$ and $I_{em}(t)$. Therefore, the above model of PEM-HEH governed by the system (5)-(10) is derived from the combination of the distributed parameter model for the cantilervered bimorph and the lumped parameter model of the subsystem including three masses $M_f, m_g,$ and M_t. As proven in (Hung et al., 2025), the system (5)-(10) has two phenomena, the first is the frequency-doubling phenomenon where the axial vibrational frequency is two times of the forced frequency, and the squared-amplitude phenomenon where the axial displacement increases four times when the excitation increases two times.

3. Phase portrait of pem-heh

3.1. Electrical and mechanical responses of PEM-HEH

Consider the transverse displacement $w_{rel}(x,t)$ is estimated by the single-mode expression as:

$$w_{rel}(x,t)\approx\eta_r(t)\phi_r(x); \quad (13)$$

in which $\eta_r(t)$ is the modal mechanical coordinate expression, and $\phi_r(x)$ is the eigenfunction of the concerned r_{th} vibration mode

$$\phi_r=A_r\left(\cos\frac{\lambda_r}{L}x-\cosh\frac{\lambda_r}{L}x+\varsigma_r\left(\sin\frac{\lambda_r}{L}x-\sinh\frac{\lambda_r}{L}x\right)\right) \quad (14)$$

where

$$\varsigma_r=\frac{h_2(\sin\lambda_r+\sinh\lambda_r)-h_1(\cos\lambda_r-\cosh\lambda_r)-\sin\lambda_r+\sinh\lambda_r}{h_2(\cos\lambda_r-\cosh\lambda_r)+h_1(\sin\lambda_r-\sinh\lambda_r)-\cos\lambda_r-\cosh\lambda_r}$$

and the modal constant A_r is found by the normalization (Erturk and Inman, 2011)

$$YI\int_0^L\left(\frac{d^2\phi_r(x)}{dx^2}\right)^2dx=\omega_r^2 \quad (15)$$

At the short-circuit resonance frequency and simultaneous resonance conditions of two harvesters and ignoring the direct interactions between the axial and base motions, after some manipulations the system (5)-(10) can be transformed to a dimensionless one as follows

$$\ddot{\eta}_n+\eta_n+2\zeta_r\dot{\eta}_n-v_P+2\phi_2(u_n\ddot{\eta}_n+\dot{u}_n\dot{\eta}_n)+\phi_1\ddot{u}_n\eta_n=\sigma_n\sin\tau \quad (16)$$

$$\ddot{u}_n+4(\zeta_m+\zeta_e)\dot{u}_n+4u_n+\phi_1\eta_n\ddot{\eta}_n+(\phi_1-\phi_2)\dot{\eta}_n^2=0 \quad (17)$$

$$\dot{v}_n+\frac{v_p}{\upsilon_r}+\gamma_r\dot{\eta}_n=0 \quad (18)$$

$$\tau=\omega_r t,\tilde{\omega}=\frac{\omega}{\omega_r},\eta_n=\frac{\eta_r}{W_0\sqrt{M_t}},u_n=\frac{u}{W_0},\zeta_r=\frac{c_s\omega_r}{2Y},\zeta_m=\frac{c_m}{2\sqrt{kM_t}},\alpha=\frac{\sqrt{k/M_t}}{\omega_r}$$

where $v_n=\frac{\theta_p v_p}{\omega_r^2W_0\sqrt{M_t}}\frac{d\phi_r}{dx}(L),\upsilon_r=2R_lC_p\omega_r,\gamma_r=\frac{\left(\theta_p\frac{d\phi_r}{dx}(L)\right)^2}{2C_p\omega_r^2},\zeta_e=\frac{\theta_{em}^2}{2R_{l1}\sqrt{kM_t}},$ (19)

$$\phi_1=W_0M_t\left(\phi_r(L)\frac{d\phi_r}{dx}(L)-\int_0^L\left(\frac{d\phi_r}{dx}\right)^2dx\right),\phi_2=W_0M_t\frac{d\phi_r}{dx}(L)\left(L_0\frac{d\phi_r}{dx}(L)+\phi_r(L)\right),$$

$$\sigma_n=\frac{1}{\sqrt{M_t}}\left(m\int_0^L\phi_r(x)dx+(M_t+M_f+m_gL_g)\phi_r(L)+\left(M_tL_0+\frac{m_gL_g^2}{2}\right)\frac{d\phi_r}{dx}(L)\right)$$

Due to the frequency-doubling phenomenon, the solution of the system (16)-(18) is assumed to be

$$\eta_n = A_\eta \cos(\tau + \varphi_\eta), u_n = A_u \cos(2\tau + \varphi_u), v_n = A_v \cos(\tau + \varphi_v) \quad (20)$$

where the amplitudes and phases of the mechanical and electrical responses can be expressed in the forms of unknown coefficients $u_s, u_c, \eta_s, \eta_c, v_s, v_c$

$$A_\eta = \sqrt{\eta_s^2 + \eta_c^2}, \quad A_u = \sqrt{u_s^2 + u_c^2}, \quad A_v = \sqrt{v_s^2 + v_c^2}$$
$$\varphi_\eta = a\tan(\eta_s / \eta_c), \varphi_u = a\tan(u_s / u_c), \varphi_v = a\tan(v_s / v_c) \quad (21)$$

Using the harmonic balance method, these coefficients can be determined from the following equations (Hung et al., 2025)

$$(2\phi_1 - \phi_2)u_c\eta_s - 2\zeta_r\eta_c - (2\phi_1 - \phi_2)u_s\eta_c - v_s = \sigma_n \quad (22)$$

$$2\zeta_r\eta_s - (2\phi_1 - \phi_2)u_s\eta_s - (2\phi_1 - \phi_2)u_c\eta_c - v_c = 0 \quad (23)$$

$$8(\zeta_m + \zeta_e)u_c + (2\phi_1 - \phi_2)\eta_s\eta_c = 0 \quad (24)$$

$$8(\zeta_m + \zeta_e)u_s + (2\phi_1 - \phi_2)\frac{\eta_s^2 - \eta_c^2}{2} = 0 \quad (25)$$

$$-\gamma_r\eta_c - v_c + \frac{v_s}{\upsilon_r} = 0 \quad (26)$$

$$\gamma_r\eta_s + v_s + \frac{v_c}{\upsilon_r} = 0 \quad (27)$$

These are algebraic equation system which can be solved numerically, then the electrical and mechanical responses of PEM-HEH (20) can be fully determined.

3.2. Experiment of PEM-HEH

Table 1. Parameter's values in experiment

Parameter	Values
L, b, L_0, L_g, h_s, h_p (mm)	80, 30, 84, 100, 0.2, 0.2
Y_s, $\bar{c}_{11}^E$ (GPa)	112, 56
$\bar{e}_{31}$ (C/m^2)	−11.27
M_f, M_t (gr)	5, 63.55
m, m_g (gr/mm)	0.143, 0.222
$\bar{\varepsilon}_{33}^S$ (F/m)	3400ε$_0$
ρ_s, ρ_p (kg/m^3)	8780, 7500

In the paper, we concentrate on the verification of the stability of the solution η_n given by (20). To do this a simple experiment is built as shown in Figure 2. The operation of PEM-HEH in resonance with low-frequency harmonic base excitation is of interest. The input parameters are given by Table 1.

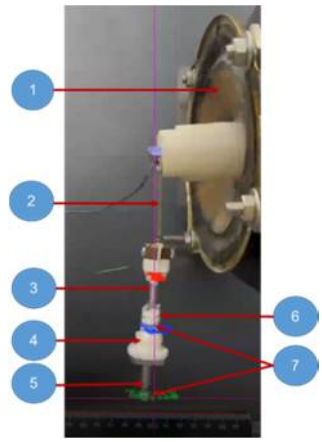

Figure 2. Experiment setup

1. Base exciter, 2. Bimorph piezoelectric beam, 3. Spring active coils,4. Movable tip mass, 5. Guide rod, 6. Spring, 7. Markers for image processing

As shown by (2), the base displacement amplitude $W_0 = 5.15$ is expressed in *mm*, the excitation frequency $f = 2\pi / \omega$ is expressed in Hz. The frequency analyses detect the natural frequencies of the transverse motion of the bimorph about 2.85Hz. Figure 3a,b,c depict the phase portrait of the bimorph tip, i.e. the relationship between transever displacement w_L and velocity $\dot{w}_L$, meanwhile Figure 4a,b,c depict the phase portrait of the movable mass, i.e. the relationship between axial displacement u and velocity $\dot{u}$.

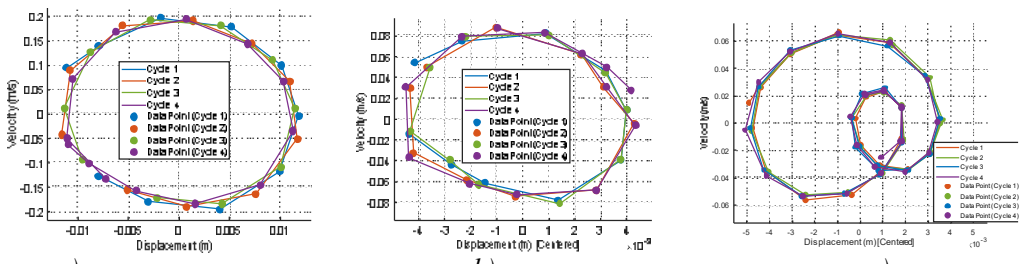

a) *b)* *c)*

Figure 3. Phase portraits of the bimorph tip with various excitation frequencies:
a) resonance regime f=2.85Hz, b) post-resonance regime f=3.16Hz, c) pre-resonance regime f=1.5Hz

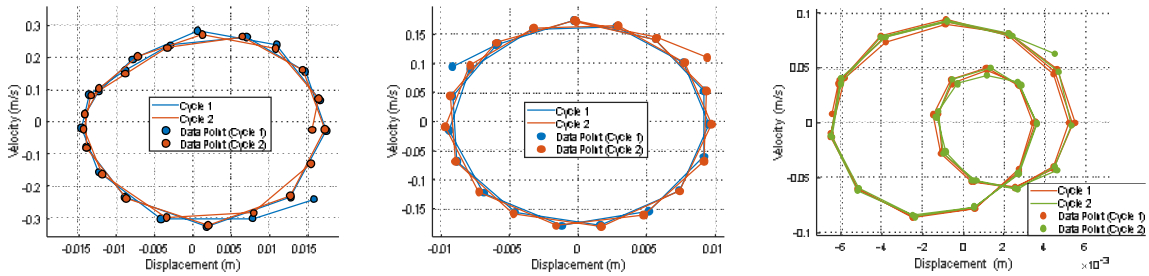

Figure 4. Phase portraits of the movable mass with various excitation frequencies:
a) resonance regime f=2.85Hz, b) post-resonance regime f=3.16Hz, c) pre-resonance regime f=1.5Hz

As seen in Figure 3a and Figure 4a, it is demonstrated the doubling frequency effect of the spring-mass-cantilevered bimorph system in resonance regime $f = 2.85Hz$ where the excitation frequency matches the natural frequency of the bimorph. When the bimorph oscillates in two periods, the movable mass oscillates in four periods. Both oscillations achieve a steady-state condition in forced vibration with maximum amplitude, i.e. $w_{L\max} = 10mm, u_{\max} = 15mm$, and maximum velocity, i.e. $\dot{w}_{L\max} = 0.2m/s, \dot{u}_{\max} = 0.3m/s$. The phase trajectory approximates an ideal ellipse, indicating the oscillation is close to that of a damped harmonic oscillation characterized by a phase lag between displacement and velocity, about $\pi/2$, and the energy transfer efficiency is maximum. The closed orbit confirms an absolute energy balance between the excitation source and the damping forces.

As shown in Figure 3b and Figure 4b, the system operate in post-resonance regime $f = 3.16Hz$. The system returns to a stable, closed-orbit steady-state. The amplitude and velocity reductions compared to resonance are due to the dominance of the inertial forces of the attached mass, i.e. $w_L = 4mm, u = 10mm$ and $\dot{w}_L = 0.08m/s, \dot{u} = 0.17m/s$. The trajectory is rounded indicating a larger phase lag between displacement and velocity, approaching π, which significantly reduces the energy transmission efficiency. Generally, it can be emphasized that the periodic solutions given by (20) are good approximations for two cases of resonance regime and post-resonance regime where there is a stable equilibrium point.

In pre-resonance regime $f = 1.5Hz$, as illustrated in Figure 3c and Figure 4c, it is also observed a large reduction in amplitude and velocity, i.e. $w_L = 3mm, u = 5mm$ and $\dot{w}_L = 0.06m/s, \dot{u} = 0.09m/s$. The diagram illustrates the superposition of the transient response and the steady-state sesponse. This superposition results in a distorted, temporarily helical trajectory. The presence of such a complex, non-elliptical path suggests the dominance of the transient response s and/or contributions from higher harmonics related to nonlinearity. The smaller amplitude and velocity reflect poor energy transmission efficiency. Hence, the periodic solutions given by (20) are no longer suitable to illustrate this quasi-periodic behavior where the system has more than one equilibrium point.

4. Conclusion

The main objective of this paper is to investigate the characteristics of nonlinearity of a nonlinear piezoelectric-electromagnetic hybrid energy harvester (PEM-HEH). A sample test of PEM-HEH is performed. To visualize the oscillatory behavior of PEM-HEH, phase portraits involves plotting the system's position against its velocity is conducted. The transverse motion is optimized as usual while the axial one is optimized by the frequency doubling effect. The natural frequencies of the transverse and axial motions respectively should be tuned to be near the excitation frequency and near twice the excitation frequency.

The responses of the bimorph and movable mass in phase portraits are of interest. It is shown that in resonance and post-resonance regimes, say the excitation frequency is $f = 2.85Hz$ and $f = 3.16Hz$, respectively, the phase trajectories are stable, closed-orbit ellipse, which indicates steady-state oscillations. The periodic solutions are good approximations for these two regimes with a stable equilibrium point. Meanwhile, in pre-resonance regime, i.e. the excitation frequency is $f = 1.5Hz$ the phase trajectories become distorted, temporarily helical, and it requires a quasi-periodic solution to describe insight into this nonlinear effect with more than one equilibrium point.

It underscores the need for further development of solution methods to fully analyze this nonlinear hybrid energy harvesting system, as well as similar electromechanical systems.

Acknowledgments

The authors acknowledge the support by Thuyloi university under grant number 83/HĐ-ĐHTL according to the decision number 2018/QĐ-ĐHTL 07/7/2025.

References

Ahmad M. M., Khan F. U. (2020), *"Review of vibration-based electromagnetic-piezoelectric hybrid energy harvesters",* International Journal of Energy Research, p1-40, doi:10.1002/er.6253.

Erturk Alper and J. Inman Daniel (2011), *"Piezoelectric Energy Harvesting"*, John Wiley and Sons.

Fan Yimin, Niu Mu-Qing, Ghayesh Mergen H., Amabili Marco, Chen Li-Qun (2024), "*Nonlinear vibration energy harvesting via parametric excitation: Snap-through with time-varying potential wells",* Mechanical Systems and Signal Processing, 220, 111625, doi.org/10.1016/j.ymssp.2024.111625.

Fang S., Zhou S., Yurchenko D., Yang T., Liao W. H. (2022), *"Multistability phenomenon in signal processing, energy harvesting, composite structures, and metamaterials: A review"*, Mechanical Systems and Signal Processing, 166, 108419, doi.org/10.1016/j.ymssp.2021.108419.

Zheng R., Nakano K., Hu H., Su D., Cartmell M. P. (2014), *"An application of stochastic resonance for energy harvesting in a bistable vibrating system"*, Journal of Sound and Vibration, 333(12), p2568–2587, doi:10.1016/j.jsv.2014.01.020.

Li P., Gao S., Niu S., Liu H., Cai H. (2014), *"An analysis of the coupling effect for a hybrid piezoelectric and electromagnetic energy harvester"*, Smart Materials and Structures, 23(6), 065016, doi:10.1088/0964-1726/23/6/065016.

Hung, N. N., Viet, L. D., Linh, N. N. (2025). "*On a doubled-frequency squared-amplitude hybrid energy harvester"*, *International Journal of Non-Linear Mechanics, 178*, 105192, doi.org/10.1016/j.ijnonlinmec.2025.105192.